20FUN04 PrimA-LTD

D2: Report describing the influence of different decay schemes of radionuclides (such as pure electron-capture of ^{55}Fe, β/γ-decay of ^{129}I or α/γ-decay of ^{241}Am) on activity standardisation and the requirements for statistical uncertainties < 0.1 % using low temperature detector-based spectrometers

Lead partner: PTB

Due date of the deliverable: 30 November 2022

Actual submission date of the deliverable: 3 February 2023

This project has received funding from the EMPIR programme co-financed by the Participating States and from the European Union's Horizon 2020 research and innovation programme.

EMPIR EURAMET
The EMPIR initiative is co-funded by the European Union's Horizon 2020 research and innovation programme and the EMPIR Participating States

Table of contents

Section A: Introduction

An important task in several disciplines, including nuclear physics, medical imaging and environmental monitoring, is the determination of the activity of the radionuclides used for these applications. The established standardisation techniques to measure the activity of samples containing radionuclides make use of different types of detectors. These include proportional, liquid scintillation and internal gas counters, as well as semiconductor detectors like HPGe detectors and scintillation crystals like NaI(Tl). These types of detectors detect the energy, which is deposited by particles emitted by radioactive decays via ionization and excitation of the atoms and molecules inside the materials of which the detectors are made of. This can lead to relatively poor energy resolutions of up to a few keV and thus, also in high energy thresholds of a few tens of keV. This is by far not a problem for most of the used radionuclides due to their, compared to the threshold, high decay energies. However, activity determination of nuclides with low decay energy can strongly be affected by the poor energy resolution. As a result, the activity determination of low energetic decaying nuclides is strongly model dependant, which leads to high uncertainties.

Low temperature detectors like magnetic microcalorimeters (MMCs), which are primarily used for X-ray and alpha particle spectroscopy, have a high energy resolution of up to a few eV. Since a few years, research is applied to adapt MMC-based detectors for metrological use-cases such as the precise determination of decay data. By depositing the source material into the MMC absorbers, i.e., in a 4π geometry, very low energy threshold of less than 100 eV and very high particle detection efficiency of up to 100 % could be achieved to improve the activity standardization of certain radionuclides like for the pure EC radionuclide Fe-55.

In this report, we describe how low temperature detectors, especially MMCs, could be used to precisely measure activities. For this, we describe which effects are expected on the activity determination for different decay schemes. We also describe the influence of detector physics and signal and data processing on the activity determination.

Section B: Influence of decay physics on activity determination with low temperature detectors

B1 Decay schemes

Generally, there are three types of radioactive decays, namely alpha decay, beta decay and electron capture. The type of decay needs to be accounted for, when determining the activity of a sample, because of the different effects on the detector, especially detection efficiency, coincident decays and the expected number of events per decay, especially for meta-stable states. We will discuss the expected effects in the following chapter for the three named decay modes.

B1.a Alpha decay

One good reason for using low temperature detectors for activity determination of alpha decaying nuclides is that alpha particles can be easily absorbed with 100 % efficiency by using gold absorbers with a thickness of a few micrometers. For example, an alpha particle with an energy of 4 MeV can be stopped by using approximately 7 µm of gold [1].

In alpha decay, an alpha particle is emitted with an energy of a few MeV, the nuclei and the atoms being excited, gamma-rays, X-rays and electrons are almost simultaneously emitted (excepted for isomeric states). The energies of the emitted alpha particles are discrete. This means by applying an energy threshold below the minimum possible alpha energy (e.g., ~ 1 MeV), it is possible to count all alpha-caused events while reducing background efficiently. Even if low-energy gammas and X-rays from the decay are measured in coincidence with the alpha particles, the performance is not reduced, because the resulting total deposited energy is still higher than the energy deposited by the alpha particles alone and thus still above the energy threshold.

In the energy region above a few hundred keV, the absorption probability for gammas is close to zero. For instance, when using 7 µm of gold, the probability to absorb a photon with an energy larger than 150 keV is smaller than 0.2 %, and the probability to absorb photons with energies above 1 MeV is less than 0.1 % [2]. This means that only alpha particles will deposit energy in the detector, as well as low-energetic X-rays and gamma rays which can only deposit energy in coincidence with the alpha particles. This way, background due to X-rays and gammas emitted from the surrounding is reduced, which leads to an improvement of the accuracy and precision of activity measurements.

In principle, electrons with energies above a few hundred keV emitted by any source except the radionuclide of interest can result in a background for the activity determination. Possible sources could be beta decaying nuclides, knock-on electrons produced by muons in the set-up materials and internal conversion electrons emitted after certain radioactive decays.

Using low temperature detectors to determine activity can reduce uncertainties significantly. Due to the high energy threshold of the detectors, only alpha particles will deposit energies above threshold in the detector (including coincident electrons, low-energy X-rays and gammas). This model-independent approach can help to reduce the impact of uncertainties on the measurement results.

However, it is important to note that if the start nuclide is part of a decay chain, all alpha particles emitted by all alpha-decaying nuclides in the decay chain will be measured. In this case, the uncertainty may not be close to zero, as knowledge of the decay chains and branching ratios is needed to determine the activity of each nuclide in the chain. In order to reduce this uncertainty, the high energy resolution and the spectrometry capabilities of the MMCs can be used to identify the abundance of nuclides in the decay chain. With spectrometry, it is also possible to determine the activity of each nuclide based on the well-known energies of the emitted alpha particles. Nevertheless, the uncertainty on the activity determination of the alpha-decaying fraction of the decay chain should still be close to zero. This is because the high energy threshold of the detectors means that the background level can be assumed to be negligible above 1 MeV and is not existent above 2.6 MeV (the highest naturally occurring gamma line from Tl-208). As a result, the statistical uncertainty in the measurement can be calculated using the standard deviation of a Poisson distribution without the need for corrections.

B1.b Beta decay

In case of beta decaying radionuclides, the inefficiency for beta particles with energies below the smallest trigger threshold energy possible of approximately 100 eV for MMCs [3, 4, 5, 6] must be corrected by theoretical models. These models vary from one to another, particularly at energies below a few keV [5, 7, 8], which can introduce a degree of uncertainty into the measurement. In addition, the measured shape of the beta spectrum may not match the predicted shape according to theory due to energy losses of beta electrons through the process of Bremsstrahlung [9]. This can be mitigated to some extent through the use of smart detector geometries and material choices, such as using as large as needed and as small as possible absorbers made of materials with a high atomic number. Alternatively, the radionuclides can be embedded in a material with a small atomic number to reduce the amount of Bremsstrahlung produced. Still, the material with a small atomic number needs to be surrounded by a high mass number material to absorb X-rays efficiently.

To further improve the accuracy of the measurement, the measured beta spectrum can be unfolded (corrected) using Monte Carlo simulations. However, this correction is only possible to a certain extent (e.g. above the energy threshold), and the resulting uncertainty depends on the used model [9]. Because electron-caused events are counted always, if enough energy is deposited by them, the activity determination of nuclides beta-decaying to daughters with many excited states should also easily be possible. On the other hand, for spectrometry, they present challenges, as the resulting beta spectra may be difficult to separate from each other.

When using low temperature detectors for activity determination of beta decaying nuclides, not all decays are counted because missing counts below the threshold occur. This should only cause a minor effect, since it depends on the fraction of the beta spectrum below the threshold that can be corrected using theoretical models. The ability to analyse the spectral shape can help to minimize the influence of background lines on the determination of activity, as they can identified and removed.

B1.c Electron Capture

One characteristics of electron capture spectra measured in 4π geometry is that they consist of lines rather than of continuous spectra. Depending on the position of the threshold and the location of the lines, by varying the energy threshold, a significant portion of the spectrum can be included or excluded. This can significantly alter the uncertainty of the measurement, as the part of the spectrum below the energy threshold, which is not measured, must be corrected using theoretical models. It is important to note that these models may not always agree with each other, leading to potential sources of uncertainty in the measurement [10,11].

However, another characteristic of EC spectra is that the intensity of lines decreases at lower energies. This means that the effect of the energy threshold may be less significant at lower energies, as the intensity of the lines becomes smaller.

The presence of background lines can also impact the accuracy of activity determination using EC nuclides. If background lines are located in close proximity to the EC lines, they can significantly affect the reconstructed activity of the sample. However, if the background lines are well separated from the EC lines, they can generally be easily distinguished and removed from the EC spectrum. This can help to improve the accuracy of the activity determination by reducing the impact of background on the measurement [11].

Section C: Influence of detector physics on activity determination with low temperature detectors

C1 Absorption efficiency

Generally, low temperature detectors have very small thickness of the order of 10 µm to 100 µm. According to [1], alpha particles are fully stopped in a 10 µm thick gold film, if they have energies smaller than approx.1.5 MeV, or less than 7 MeV for a 100 µm film respectively. In this energy range, alpha particles mainly lose energy by ionization (until they reach energies of a few keV, where nuclear recoil dominates). Thus, many knock-on electrons (delta radiation) are produced [12].

Electrons with energies smaller than approx. 80 keV are fully stopped in 10 µm of gold, while a thickness of 100 µm is needed to fully stop electrons with energies of less than 350 keV [1]. However, in contrast to the highly charged and heavy alpha particles, electrons not only lose energy by ionization, but also by producing Bremsstrahlung. For instance, an 80 keV electron transfers about 1 % of its energy into Bremsstrahlung, while a 350 keV electron transfers about 3 % of its energy in Bremsstrahlung [1].

In contrast to charged alpha particles and electrons, the absorption probability of photons in very thin detectors is much smaller. In gold and in the energy region of less than 100 keV, photons predominantly lose energy by the atomic photoelectric effect. In this energy region, the photons deposit their complete energy, if they interact with the material. In the energy region of 100 keV to 1 MeV, Compton scattering dominates [12]. This means, regardless of the energy, the probability is not zero for X-radiation and Bremsstrahlung escaping the absorber undetected. For instance, the probability that a 10 keV photon is stopped in 10 µm of gold is about 89 % and 9 % for 100 keV photons [2]. In 100 µm of gold, the probabilities to absorb the photons are much higher. In this case, the probability to absorb 10 keV photons is close to 100 % and about 62 % for 100 keV photons.

While for detecting alpha particles, the absorber thickness is sufficient to be 10 µm, for electrons and photons the detection efficiency will strongly depend on the particle energy, and thicker absorbers are used for instance. However, the FWHM energy resolution and the energy threshold of cryogenic detectors increase with the absorber heat capacity. Therefore, a compromise is required to achieve high energy resolution and high detection efficiency. Monte Carlo codes are a useful tool to size the minimal dimensions of the absorber for a desired detection efficiency and achieve the best energy resolution. It is why the required geometry and size of the absorbers for a high efficiency are determined by Monte Carlo simulations.

The detection efficiency in a 4π geometry will also depend on the decay scheme of the radionuclide and not only on the particle energies. Indeed, with the exception of pure beta emitters, most of the other radionuclides decay to an excited atom and/or nucleus, thus if one of the particles is not absorbed, other particles can be detected, and the disintegration will be counted in the spectrum. Even if a radionuclide emits high-energy gamma radiation that is difficult to absorb, it is not necessary to size the absorber accordingly. The gamma will be emitted in coincidence with other particles, e.g. alpha particles or electrons, which can be absorbed instead. Also, the absorbers can be designed in such a way that the host material of the source differs from the absorber material. Thus, a material with a low atomic number can be used as host material, so that less Bremsstrahlung is generated because the cross section for creating Bremsstrahlung increases with the atomic number. However, the absorber material should have a high atomic number, so that X-radiation and Bremsstrahlung can be detected more efficiently. For instance, this effect was studied for the beta-decaying Cl-36 with a maximum beta energy of about 710 keV. Monte Carlo simulations based on EGSnrc [13] were performed by simulating mono-energetic electrons with energies of 750 keV in gold foils with dimensions of 600 µm × 3.1 mm × 3.1 mm (see Figure 1). By adding a copper layer to the gold foil without increasing the total volume, the energy loss due to escaping Bremsstrahlung is reduced by more than 50 %.

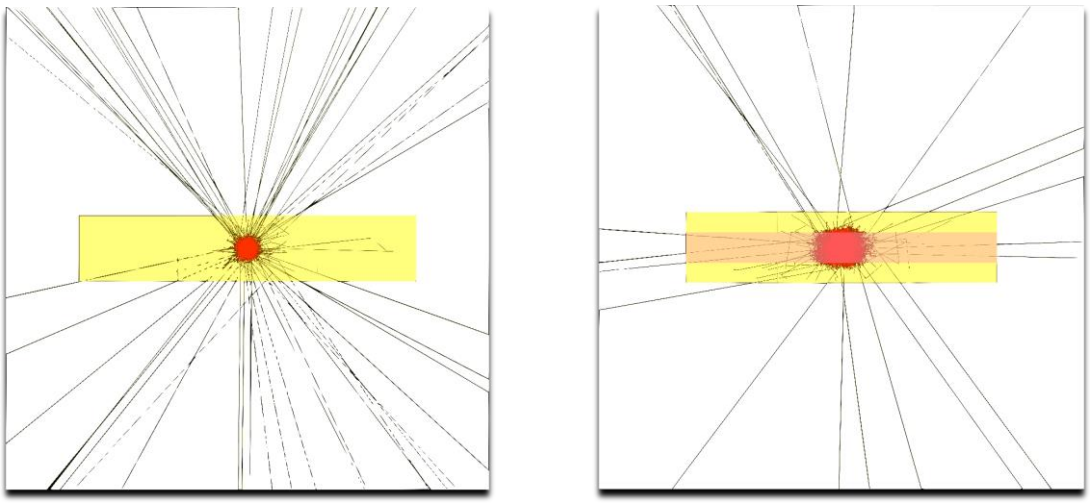

Figure 1: Particle propagation paths resulting of EGSnrc-based simulations. The electron paths are shown in red and the photon (Bremsstrahlung) paths in black. Left: 750 keV electrons start in the centre of a gold foil (yellow coloured) with dimensions of 600 µm × 3.1 mm × 3.1 mm. Right: 750 keV electrons start in the centre of a copper layer (orange coloured) with dimensions of 200 µm × 3.1 mm × 3.1 mm, which is between two gold foils with dimensions of 100 µm x 3.1 mm x 3.1 mm each. While the mean free path for electrons is larger in copper than in gold, less photons leave the volume with the addition copper layer.

C2 Background radiation

Due to the relatively slow signals with decay times in the order of a few milliseconds, the activity per pixel should not be higher than a few Becquerel. Otherwise, the pile-up rate would be too large. If we aim for an uncertainty of 0.1 % on the determined activity and thus on the number of observed counts, methods to identify and estimate any background source is mandatory. In the following, we will discuss three possible background sources, namely radiation caused by muons, possible naturally occurring radionuclides in the materials used for the set-up and contamination in the source materials. In the following and for simplicity, we assume a count rate of about 10^6 decays per day per pixel, which can be achieved with an activity concentration of about 12 Bq per pixel. There are several sources of background that are discussed in the following sections. But – as it is common practice in radionuclide metrology anyway – dedicated background measurements are carried out to quantify the background and apply corrections correspondingly.

C2.a Muon-generated radiation

The muon flux at sea level is approximately 180 muons s^{-1} m^{-2}, which can vary by about 10% depending on the time and location [12]. This means that about 16 muons pass through a MMC absorber (pixel) with an area of 1 mm × 1 mm in a single day. This can also be expressed in 1.85×10^{-4} muons $pixel^{-1}$ s^{-1}. In this example, this is roughly 1.6 % of the total background. The impact of muonic background can be reduced by taking into account the amount of energy deposited by muons and muon-generated secondary radiation, which follows the Landau distribution [14, 15].

Monte-Carlo simulations and calculations in previous studies have shown that the muonic background can be fully suppressed for alpha-decaying radionuclides with energy thresholds above 1 MeV, since the energy deposited by muons is in the order of a few 10 keV. For medium energy scales, e.g., observed using beta-decaying radionuclides, the muonic background should be fully considered. In the case of low energy scales, such as those observed in electron capture radionuclides, the muonic background is reduced [15]. However, it is important to note that muons and muon-generated secondary radiation do not only deposit energy directly in the detector pixels, but also in the substrate adjacent to the pixels. In previous studies it was observed that pulses induced by such events can occur more frequently than direct hits (about 10 times as often), although the reconstructed energies of these events are typically less than 1 keV and therefore may not be relevant, especially for alpha-decaying radionuclides.

The total muonic background can make up to 16 % of the maximum background counts. It can further be reduced with the use of pulse shape discrimination methods, by dedicated background measurements, with the use of shielding or by information from coincidences among pixels (if arrays of MMCs are used).

C2.b Naturally occurring radionuclides in the setup

Naturally occurring radionuclides like U-238, Th-232 and their daughters can be found in metals with typically activity concentrations in the range of 0.1 mBq / kg for pure metals to 1 Bq / kg for alloys [16, 17, 18]. Monte Carlo simulations have been used to study the effect of such radionuclides on the measured energy spectrum of low temperature detectors, such as MMCs with sizes of 0.2 mm × 0.2 mm. The simulations show that for an activity concentration of 1 Bq / kg in the metallic materials surrounding the MMCs, less than 2×10^{-2} counts pixel^{-1} day^{-1} are expected in the first 100 keV. The activity concentration in the printed circuit board located in close proximity to the MMCs may reach activity concentration levels of up to 1 kBq / kg. However, due to the small solid angle, it is expected that less than 0.2 counts pixel^{-1} day^{-1} will be counted in the first 100 keV due to activity in the circuit board. Overall, even when using MMCs with sizes of several square millimeters, naturally occurring radionuclides should not significantly affect the activity determination [19].

C2.c Radioactive contaminants in the source material

The production of radionuclides inherently comes with the risk or even the expectation of radioactive contaminants in the source material. Chemical and mass separation can be used to remove contaminants. While chemical separation is regularly used, although it cannot remove contaminants of isotopes of the same element, mass separation can separate isotopes, but is very complex and requires dedicated large-scale facilities. In addition, knowledge and experience to run these facilities are needed and is therefore only used in very specific circumstances that justify the large effort.

Most of the time, especially for activity determination, it is sufficient to identify contaminants and their relative quantity and apply corrections to the results accordingly. Identification is usually done by gamma and X-ray spectrometry in dedicated measurement set-ups, but in case of MMCs, the measured spectrum can also be used to identify contaminants. Especially for low energy EC decays, this is often the best option because of the good energy resolution of MMCs, that is usually at least one order of magnitude better than other detectors usually used to identify contaminants in that energy range.

Nevertheless, some contaminants, e.g. pure β-decaying nuclides, are very hard to identify and need to be handled similar to unidentified background, instead of identified contaminations.

C3 Crosstalk between detector channels

In principle, there are two types of crosstalk, that are relevant for MMCs. Since MMCs are thermal detectors, heat transfer between sensors can generate a signal in a secondary channel. The second type is concerned with the read-out chain, starting with the read-out SQUID-sensors, the cryostat wiring to the room temperature analogue electronics operating the MMC/SQUID combination, followed by the analogue-to-digital conversion.

In the current MMC designs, one chip hosts only a single read-out channel, therefore, thermal crosstalk between channels is basically eliminated, since crosstalk due to heat transfer is dominated by heat transferring through the chip substrate. In addition, each channel consists of two pixels in a gradiometric geometry, which are connected to the same SQUID-sensor. The two pixels of each channel generate signals with opposite polarities, of approximately the same absolute signal heights with respect to each other. Therefore, the signals of a simultaneous (local) temperature change of both pixels will cancel each other.

The analogue components of the read-out chain, i.e., the SQUID sensors and the cryostat wiring, are configured in such a way that both parasitic inductive and capacitive coupling are reduced. Firstly, the two SQUID sensor types X1NM, XS1 and XS116W (see Figure 2), to be used for the measurements within the project PrimA-LTD are of gradiometric design, so as to reduce both their sensitivity to external magnetic signals as well as inductive coupling between (neighbouring) sensors. An individual chip of the sensor type X1NM holds four independent 2nd order gradiometric SQUID sensors. The on-chip input signal leads to the sensors are configured as strip-lines, they have no practically measurable inductive coupling between from a given signal input to a neighbouring one. For the X1NM sensor as well as the XS1 and XS116W sensor types the direct SQUID-chip-to-MMC-chip wire-bond connections will be realized in a ‘cross-over’ fashion to also reduce potential inductive crosstalk of input current signals.

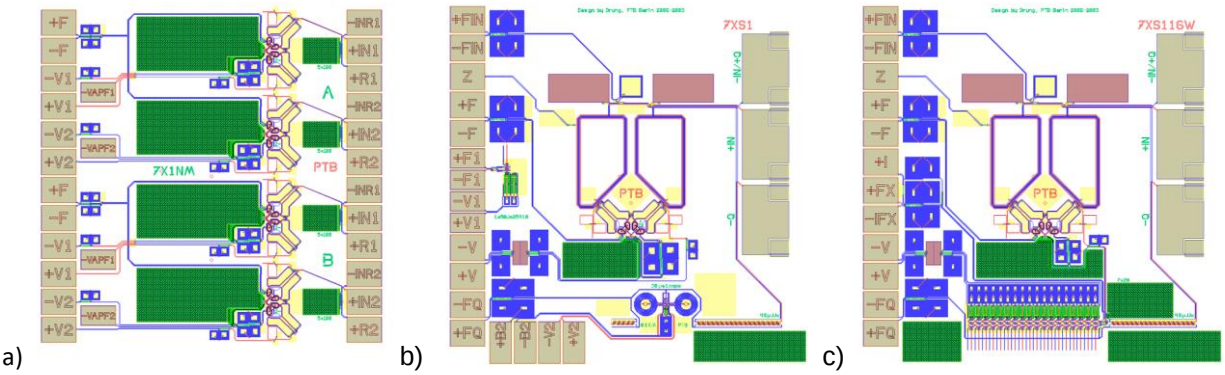

Figure 2: Chip layout of the SQUID sensor types a) X1, b) XS1 and c) XS116W to be used for the measurements within the project PrimA-LTD (chip size 3.3 mm x 3.3 mm).

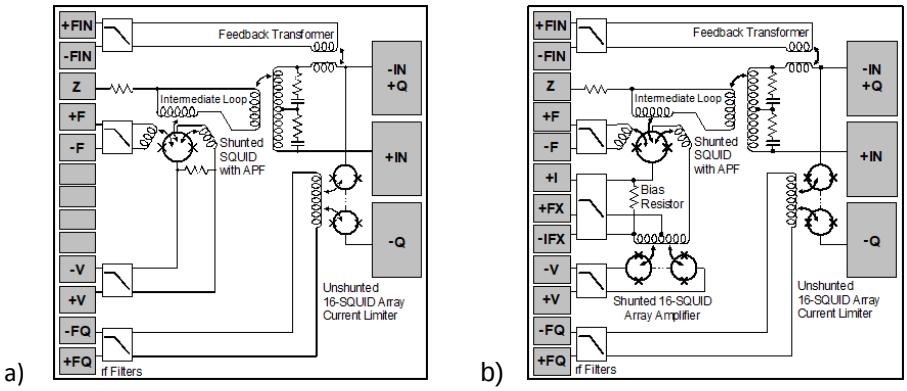

Figure 3: Circuit scheme of the SQUID sensor types a) XS1 and b) XS116W with feedback transformer.

For the sensor types XS1 and XS116W each sensor chip contains only one sensor. This increases the sensor-to-sensor distance in a multi-sensor configuration and, hence, decreases the potential for sensor-to-sensor crosstalk. Furthermore, these sensors have a double-transformer input configuration, see circuit schemes in Figure 3. Sensors of the types XS1 and XS116W can be operated such that feedback signals in response to signals from the MMC detectors are routed into the sensor input circuit. The negative feedback loop provided by the analogue electronics operating the SQUID sensors then nulls the SQUID input currents. This way, inductive crosstalk of an input signal of one SQUID channel into the input circuit of any other SQUID sensor operated in a multi-sensor measurement set-up is greatly diminished.

The cryostat wiring carries both the SQUID sensor output voltage signals to the SQUID readout electronics at room temperature as well as the (negative) feedback current signals from the SQUID electronics to the SQUID sensor. Generally speaking, capacitive crosstalk along the voltage signal leads and inductive crosstalk along the current signal leads between different SQUID channels can occur. The common way to reduce such parasitic cross-couplings is to employ twisted pair or triple wiring. Additionally, wiring harnesses can be outfitted with conductive shielding elements between signal leads of different SQUID channels that can provide further reduced crosstalk along the cryostat wiring. Here, however, thermal loading at the different temperature stages of the millikelvin refrigerator of a MMC spectrometer from such wiring harness shields need to be considered. The MMC spectrometer at PTB uses partly shielded cryostat wiring harnesses. Concluding this section, it is noted that with regards to the components of the analogue readout chain the main crosstalk-avoiding measures are to use SQUID sensors with gradiometric design as well as cryostat wiring with reduced parasitic cross-coupling along output and feedback signal leads. The multi-channel wiring of both spectrometers operated within the project PrimA-LTD implement these measures.

Section D: Influence of signal and data processing on activity determination with low temperature detectors

In contrast to the background contributions and uncertainties due to physical processes creating thermal pulses in the MMCs, here, the influence of detector noise and parasitics in the signal chain are discussed. MMCs generate continuous signals in form of voltage time traces. This raw signal requires further analysis. The signal analysis comprises analogue and digital processing steps to determine, in the final analysis, the energy spectrum or the activity of the measured sample.

D1 Signal filtering

Today, usually all data acquisition is done with analogue-to-digital converters (ADCs) and a lot of the data processing is done digitally. Nevertheless, if the detector performance is noise limited, as is the case for MMCs, the analogue signal needs to be filtered to not deteriorate the signal quality. For this, it is required to use a low pass filter at or below the Nyquist frequency, which is half the sampling rate of the ADC. Otherwise, the higher frequency parts of the signal will not be measured correctly and will appear at lower frequencies. This process is called aliasing and increases the noise level. Consequently, anti-aliasing filters are used. In special cases, mostly for spectrometry, it can be useful or necessary to use other filters as well, e.g. AC coupling or a high pass filter, but these cases will not be discussed in this report. The use of a high pass filter can lead to some undershoots that can be triggered and add some artefacts in the spectrum or in the activity determination. The use of an appropriate dead time windowing is essential to prevent this problem.

Also in subsequent digital data processing, digital filtering can be applied. It is used to optimize the signal to noise ratio (SNR), e.g. with a low pass filter to reduce the bandwidth to what is used by the decay signals. This is carried to the extreme in so-called “optimal filtering” [20], where a specialized filter function is calculated, that optimizes the SNR for a given noise spectrum and signal shape. This style of data processing is most useful for spectrometry applications, but also has its merits in activity determination, especially concerning the trigger settings and trigger threshold. I. Kim et al. [21] found that a band pass filter with optimized cut-off frequencies resulted in the best trigger performance and lowest energy threshold, and a similar approach was adopted here. In case of activity determination, it is more important to trigger as many events as possible and avoid triggering noise, and therefore an even higher threshold than five times the standard deviation of the noise (5σ), which is recommend in the mentioned work, should be applied. In our studies, we found that a 6σ threshold reaches a high enough trigger efficiency and a 7σ to 8σ threshold is needed to sufficiently suppresses accidental triggers, if no event selection is used. But since appropriate corrections to the determined activity for the trigger threshold need to be applied anyway (see Section D4), an even higher threshold can be chosen without significant drawback.

D2 Triggering and trigger threshold

Triggering is the first necessary step in identifying real detector events and allows to determine the timing of the event and start further processing. For MMCs further processing usually entails saving the signal time trace for a defined time window around the trigger event time, that can then be used in offline processing.

The two most prevalent trigger types are the leading-edge discriminator, which is also called threshold trigger in the following, and the constant fraction discriminator (CFD). A threshold trigger activates once a defined amplitude, e. g. a voltage threshold, is exceeded, while the CFD activates at a specific time in the rise time of the event in addition to an exceeded voltage threshold.

Concerning activity determination, the most important factors are the trigger efficiency (= true positive probability) and the rate of false positive events. To determine this, we conducted our own simulation study based on the pulse shape and noise characteristics (shown in Figure 4) of a recent measurement run. We generated 250000 random noise traces with 65536 samples each (corresponding to ~327 ms of acquisition time), added pulses of different amplitudes and ran different triggering algorithms on that simulated data. We used both a leading-edge discrimination and a CFD trigger, each with different voltage thresholds and three ways of dead time handling, namely no hold-off, a fixed trigger hold-off with 4096 samples and an extending dead time with a base dead time of 4096 samples. For each combination of noise trace, pulse amplitude and trigger level, we determined if the added pulse was triggered and if any additional triggers were prompted.

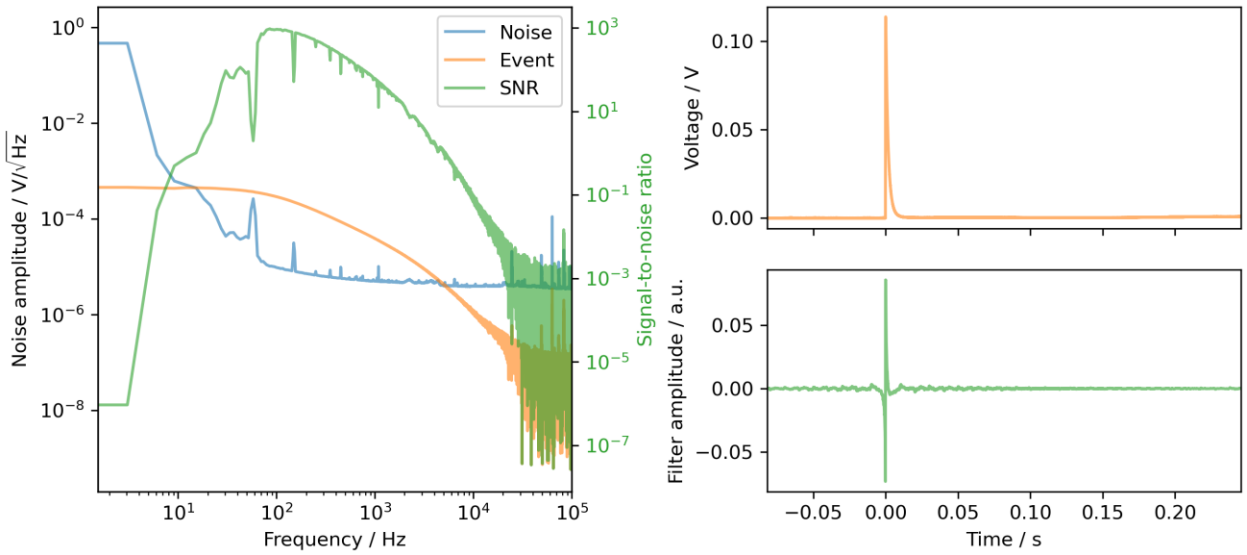

Figure 4: The data used as basis for the conducted simulation study. The noise amplitude, pulse shape and signal-to-noise ratio (SNR) in frequency space (left) and the pulse shape and the used (optimal) filter function used for data analysis in time space (right).

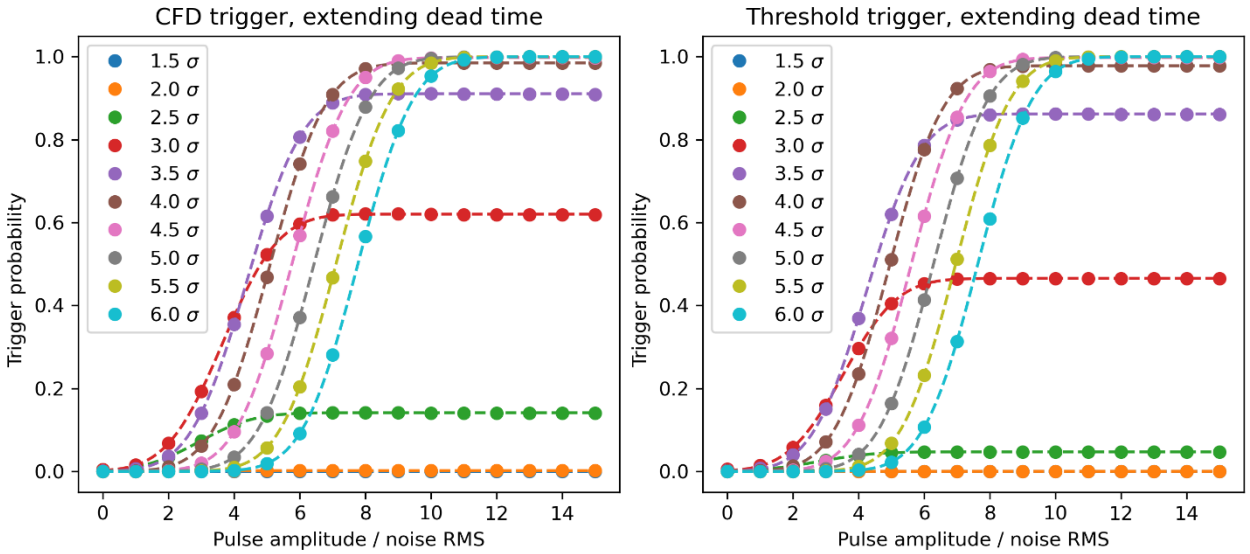

Figure 5: The trigger probability for different trigger thresholds shown at different pulse amplitudes. Both CFD trigger (left) and threshold trigger (right) are shown. In both cases an extending dead time is used.

A first aspect studied here is the trigger efficiency as a function of pulse amplitudes and how the trigger probability behaves around the trigger threshold. We define the trigger efficiency as the maximum of the trigger probability for a given threshold. The trigger probability is here given as the probability to identify the pulse positions of simulated decay events, in each time trace correctly. The simulated data also includes noise, which is calculated by using the measured noise spectrum. As can be seen in Figure 5, the trigger probability behaves like an error function with a width of about $\sigma_{err} = 1.4\sigma_{rms}$ (σ_{rms} being the root-mean-square of the simulated noise trace). At first glance, it is surprising that for low trigger levels, the probability does not reach 1. This can easily be explained when taking dead time into account. At lower trigger thresholds it becomes more likely, that noise is triggered. If the real event now lies within the dead time of previously triggered noise, the real event is not triggered and the dead time increases. The number of detected counts per live time is not affected by this, only the fraction of live time to real time is reduced. Starting at a threshold level of about 5σ, the trigger probability is nearly 100 %, which means that only a small amount of dead time is introduced. While Figure 5 only shows the results with extending dead time, a fixed trigger hold-off shows equivalent results, with slightly higher trigger probabilities at low trigger levels.

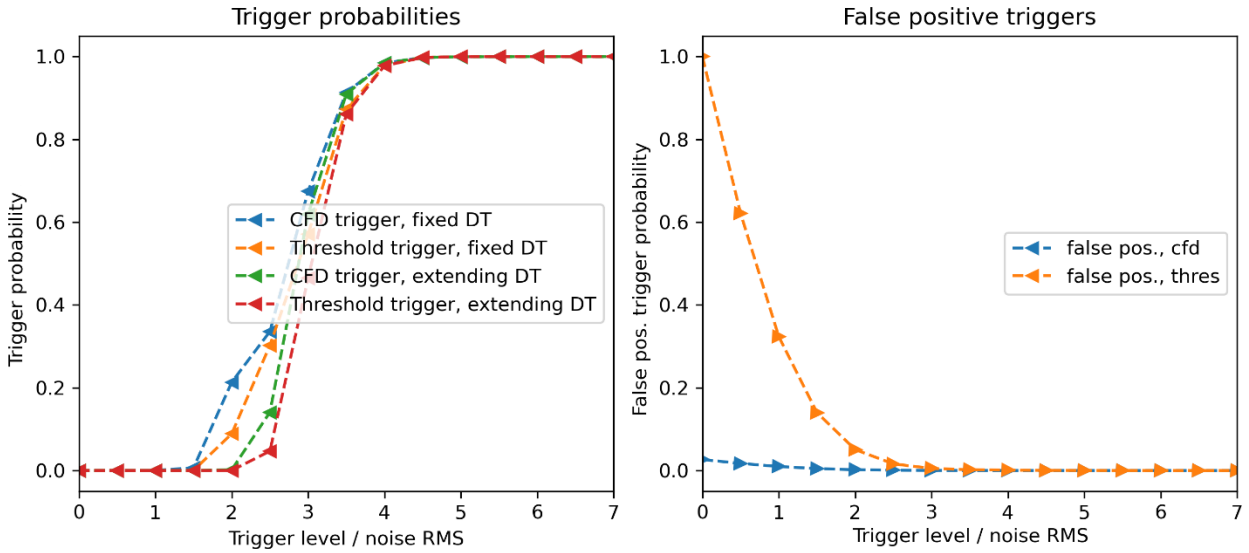

Figure 6: Trigger probability with different trigger settings (left) and rate of false positive triggers (right) at different trigger levels.

Figure 6 shows the total trigger probability with different settings for various trigger levels. The trigger probability is reduced, if the real event is within the dead time of a previous false trigger (triggered noise), which becomes much more likely when lowering the trigger level. The figure also shows the probability for false positive triggers. The first observation is, that compared to the CFD trigger, the threshold trigger shows 40 times higher false positive rates. In order to suppress the triggered noise to get a ratio of false positive triggers to true positive triggers of less than 10^{-4}, such that a total combined activity uncertainty of 0.1 % can be achieved, trigger levels of ~7σ (CFD) or ~8σ (leading edge discriminator) are required. For spectrometry measurements, these are unusually high trigger levels, but can be used for activity determination, nonetheless. On the other hand, triggered noise can easily be identified through the determined pulse shape parameters and discarded. This means that even a measurement with a trigger level of 6σ can achieve the maximum trigger probability in activity determination measurements.

D3 Analogue-to-digital conversion

The raw voltage or current time traces generated by the detectors cannot be saved or processed digitally by simply plugging the detector to a data storage or computer. First, the signals need to be digitized by using analogue to digital converters (ADCs). In order to achieve the best signal acquiring as possible, the ADC (or digitizer) has to be adjusted accordingly. The sampling rate, meaning the rate with which the input of the ADC is updated, should not be too slow. It should be adjusted such that the decay time, better the rise time, which is the faster time of both times for MMCs, is well recognizable and not limited by the sampling rate. While for the activity determination, it is primary necessary that the signal decay can be resolved and thus, the pile-up rejection window can be adjusted by the offline analysis, resolving the rise is helpful for the event selection and spectrometry channels of MMCs. The only drawback of a fast sampling rate on the other hand, is the amount of data which is generated and needed to be saved to disk. Either way, aliasing has to be considered, meaning that a low pass filter with a cut-off frequency that equals the Nyquist frequency should be applied first.

In case of MMCs, the pulse amplitudes are proportional to the energy deposited in the detector. On the one hand, the input voltage range of the ADC should be set such that the full energy range of a decay could be resolved without generating saturated pulses. For the activity determination without event selection on the other hand, saturated pulses should not be a source for high uncertainties. The same applies for the voltage offset of the ADC. It should be adjusted by considering the voltage range, the polarity of the pulses (for one or two pixels per readout channel) and the maximaum expected pulse amplitudes.

Another aspect to consider is the bit-depth of the digitizer. Commonly used digitizers have a bit-depth of 16, meaning the input voltage range is divided into 65536 bins. At first glance, this appears to be a lot. However, considering an example of measuring the full spectrum of a decay with a Q-value of 1 MeV, the binning, and thus the threshold, is reduced to 15 eV. Therefore, the very good energy resolution of a FWHM

of a few 10 eV for MMCs cannot be fully utilized. In spectrometry, a good solution is to separate the measurement in two parts by measuring the first few 100 keV of the spectrum and the high energy part of it separately. If activity determination is the main goal and separate measurements are not favourable, a single measurement of the full energy range can be performed and applying corrections for the high energy threshold, resulting from the “low” resolution of the ADC.

D4 Event selection

Event selection and classification is necessary, if MMCs are used for spectrometry. With this tool, events caused by noise, by energy deposited not only in the absorbers of the MMCs or by pile-up can be rejected by applying a selection on a pulse shape discrimination (PSD) parameter. A frequently used PSD parameter is calculated as the mean squared error of the fit between a pulse template on the pulses. However, the underlying PSD methods can depend on the energy, and the boundary between rejected and selected pulses is not always well defined, especially for the low-energy beta spectrum (compare to Figure 7).

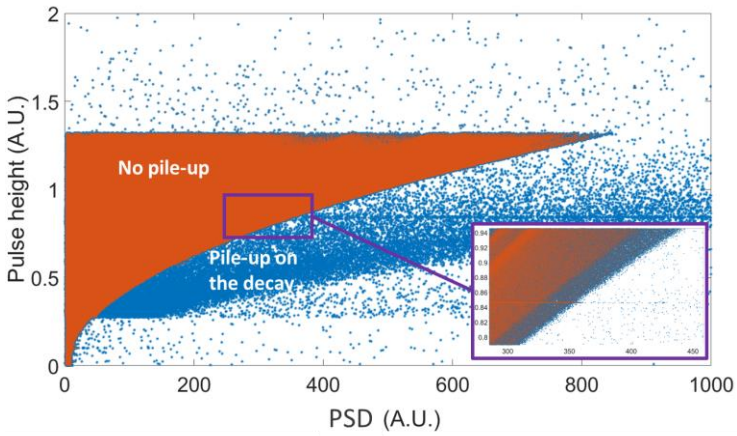

Figure 7: Pulse heights as a function of a PSD parameter calculated as the mean squared error of the fit between a pulse template on the pulses. The PSD parameter identifies the pulses with (blue) and without (red) a pile-up. The inset shows that the distinction between pulses with and without pile-up become less obvious pile-up around the selection value of the PSD parameter.

For activity determination, most critical could be the energy dependent rejection of pile-up events, which leads to an unknown behaviour of established pile-up corrections [22]. Thus, for activity determination, only a leading edge discrimination or CFD, and no further PSD, should be applied in order to use established methods to consider pile-up. On the other hand, PSD can be used for the spectrometry channel of MMC measurements to define the energy threshold precisely and thus, to reject noise effectively. Possible pulse shape parameters, which could be useful for the PSD are the rise and decay time of the pulses, the pulse’s amplitudes, the response to the matched “optimal” filter and their integral. If multiple channels are read-out simultaneously, time differences between trigger times can be used to reject noise even more [23, 24].

Section E: Activity determination with low temperature detectors

In a simplified approach, activity determination is straightforward when the detection efficiency is close to 100 %, meaning that at least one emitted particle per decay will partially deposit its energy. Nevertheless, the total deposited energy of all particles emitted in a single decay needs to be larger than the threshold to generate a counted signal. In this case, activity determination is given by $(N+N_0)/T_{\text{live}}$, where N and N_0 are the number of counts above and below the threshold respectively. T_{live} is the live time of the system. In the case of measurements of alpha-decaying samples, N_0 is 0 due to the very large deposited energies compared to the threshold. In the case of beta-decaying and EC samples, N_0 can be estimated by theoretical decay data. Alternatively, it can also be extrapolated down to zero for beta spectra. Knowing that MMC can achieve very low threshold of less than 100 eV, the ratio N_0/N is expected to be small (compare to section D2). In addition, the trigger level has to be chosen carefully. Indeed, when a threshold level is equal or below the noise level, noise triggering can produce false-triggered events, which increases the count rate and thus, the determined activity. It is preferable to set the trigger level at a level much higher than the noise limit because it is easier to correct N_0 from missing counts than to remove false events (see section D2). In addition, noise can vary, especially when data is taken over several weeks. Therefore, setting a higher trigger level will prevent noise triggering due to an unexpected noise variation.

The live time is given by $T_{\text{live}} = T_{\text{real}} - T_{\text{dead}}$, where T_{real} is the real time of data taking, and T_{dead} is the dead time. The real time is simply the stop date minus the start date of recording. It can be given by the clock of the acquisition card, which however needs a traceable time base reference, to compensate for any time drift. Additionally, for the activity determination, a reference date needs to be defined and for decay correction the start time of each measurement needs to be recorded in absolute time, e.g., UTC. It could be necessary to suppress portions of the raw data, for example due to large temperature variations of the cryostat. In this case, the dead time needs to be corrected accordingly.

In principle, the dead time T_{dead} is the time during which no pulse can be counted. Most of the dead time is driven by the decay time of the pulses, i.e. a pulse cannot or should not be counted if it falls on the decay of a previous pulse. The dead time can be determined using a non-extendable time (NEDT) or extendable dead time (EDT) [22]. A dead time window duration is chosen in order to cover the longest time of paralysis of the system (see Figure 8). The dead time window starts at each triggered event time. Compared to the use of EDT, using NEDT has the disadvantage that the live time needs to be corrected by mathematical formulae, while by using EDT the dead time is directly provided without the need of correction. However, if using EDT, the amount of dead time increases with the count rate. This in turn, decreases the counting statistics, up to the extreme case of paralysing the system. Knowing that the rate is controlled by the activity deposited in the absorbers, we consider only the use of EDT for our experiments.

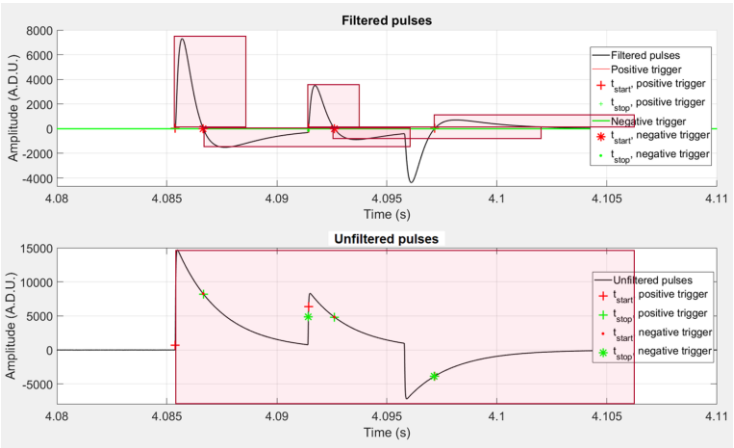

Figure 8: Example of EDT window applied on triggered pulses. Top: The stream of the pulses, which are filtered by a band pass filter, and which are detected with a trigger threshold, is shown. A dead time window is applied after each triggered event. Its duration is proportional to the duration of the signal above the trigger level. Bottom: The unfiltered pulses and the resulting dead time window corresponding to the top figure are shown.

Another contribution to the dead time is the saturation of the components in the electronics chains (amplifier, SQUID electronics or DAQ system). Saturations can lead to uncertainties on the estimation of the live time because their durations are unknown. Also, they may not be covered by a dead time window, if the dead time window was set by considering only the pulse duration. Saturations can be caused by a drift of the detector baseline due to temperature drift of the cryostat, by instabilities of the SQUID electronics working

point or by large pulses. Large pulses can also cause working point instabilities. One strategy is to limit the occurrence and the duration of saturations:

- By choosing the adequate output voltage range of each component of the electronics chain with respect to the following component input.
- By controlling the cryostat temperature to make sure that the detector baseline is stable enough (if a high pass filter cannot be used after the SQUID electronics output).
- By using the largest possible SQUID electronics bandwidth in order to gain a fast slew rate and to reduce the probability of working point instabilities.
- By applying a periodic external reset voltage to the SQUID electronics to reduce the duration of saturation due to sudden changes of the working point. This limits the maximum saturation duration to one period of the reset signal.

In addition, saturations of the ADC can be easily detected during the triggering processing of the pulses. The duration of the triggered saturation can be subtracted from the total time, or a dead time window can cover the entire saturation duration. The saturation produced by sudden changes of the working point can originate in a pulse from a decay in the absorber and cannot be corrected.

To verify that the application of the dead time is correct, it is possible to test it with simulated signals representative of an experiment. For example, we simulated signals from a MMC with two absorbers enclosing I-129 sources of 5 Bq each. The time positions of the pulses were randomly distributed in the recording period to satisfy the Poisson law of radioactive decay. The pulse heights were distributed according to the decay scheme of I-129. The polarities of the pulses were positive and negative to mimic the gradiometric geometry of the MMCs. In addition, saturations of the ADC have been introduced, both with random positions and random durations. Noise was added to the signal, which represents the detector noise. It was calculated by considering the thermal properties of the detector and the SQUID electronics noise. The simulated count rate was 10.25 s^{-1} (I-129 decays and saturations). After applying the EDT analysis, we obtained an output count rate of 10.2503(16) s^{-1}, which is in perfect agreement with the input rate, despite that the percentage of dead time to the real time (simulated) was with 38.7 % relatively high. The live time determination is therefore validated, in the case that all detected events come from decays of the source in the absorber. The activity is simply determined as the number of events with pulse heights above the threshold during the live time, minus the number of saturation events (if they are not produced by ‘real’ pulses).

However, the general case is more complex as mentioned before in section C2. Radiation produced by other origins than the source, is absorbed in the detector as well. This radiation can come from the radioactive environment, an external calibration source or radioactive impurities in the source embedded in the absorbers. Consequently, there will be a counting rate higher than the source activity. The background is composed by:

- A continuous component mainly produced by:
  - Compton scattering of photons in the environment or in the detector
  - Electrons from beta emitting radionuclides and knock-on electrons
  - Alpha particles (with reduced energies)
- Energy peaks corresponding to:
  - Fluorescence lines
  - Calibration lines: X-rays and gamma-rays
  - Escape peaks

Background peaks in the spectrum can be discriminated by energy spectrometry of the triggered events. Spectrometry analysis consists of fitting a region of interest (ROI) with functions. Some parameters are extracted from the degrees of freedom of these functions (intensities, energies, line widths etc.) and some contributions can be isolated and quantified in the spectrum. Nevertheless, changing the detector mode from counter to spectrometer has several consequences. Additional signal and data processing is required to estimate the event energy, which represented by the pulse shapes. Also, pulse selection rules have to be defined, while correcting the live time accordingly. The event energy is determined in a time window around the trigger event time. This time window comprises the pre-trigger baseline, the pulse rise

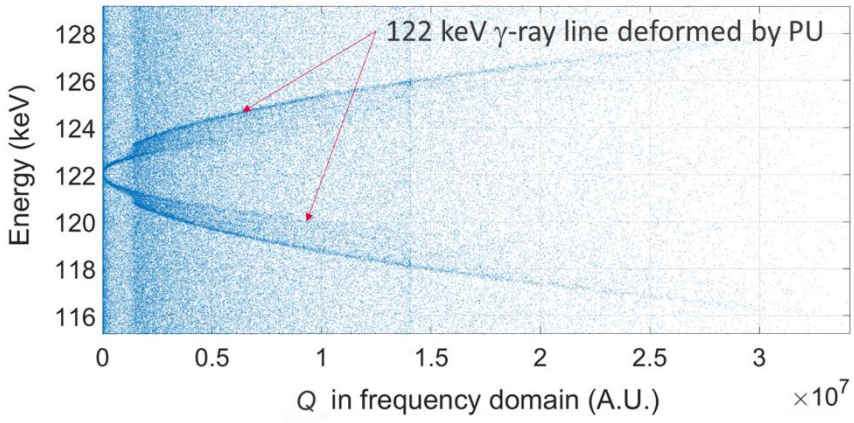

Figure 9: Estimated energies of 122 keV pulses as a function of the PSD parameter Q. Q is calculated as the mean squared error of the fit between the pulse and the template in frequency domain (optimal filtering). The drift of the lines is due to pile-ups on the decay of the 122 keV pulses.

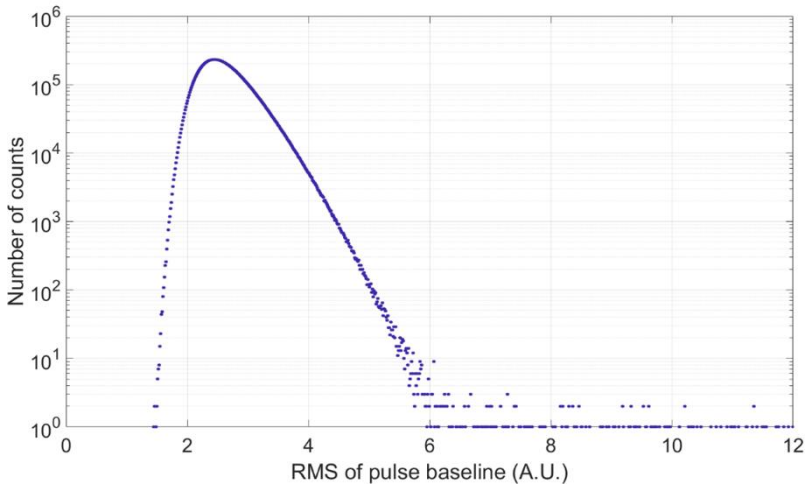

Figure 10: Root mean squares of the pulse baselines after applying an EDT. The distribution is on a relatively narrow range and does not extend at higher values than 6 meaning that pile-up on the baseline were efficiently suppressed. There are only 0.013 % of events with RMS values higher than 6.

and the pulse decay (or a portion of it). Pile-ups are pulses in addition to pulses of events of interest and can occur during the mentioned time window. They can lead to a biased energy determination and to spectrum distortions (see Figure 9). Therefore, pile-up rejection is needed. Pile-ups on the pre-trigger baseline are efficiently suppressed by EDT processing (compare to Figure 10). Rejection of pile-up on the pulse decay requires pulse shape discrimination (see section D4). Most critical are pile-ups on the pulse rise of an event of interest and are almost indistinguishable from events without pile-ups.

Rejection of time traces requires a corresponding correction of the live time. A first approximation of this correction would be to multiply T_{live} by $(1 - R)$, where R is the proportion of rejected events. More sophisticated corrections can be applied from reference [22]. Nevertheless, the uncertainty on the determined activity due to the pile-up rejection will mainly come from the criterion and the method to reject pile-up (section D4). To decrease this uncertainty, it is therefore preferable to minimize the portion of rejected pulses which can be done by applying the pulse energy determination on a smaller time window after a trigger event time. For example, a shorter pulse template can be used to fit the pulse and determine its energy, or a strong band-pass filter can be applied to determine the energy by the pulse maximum. However, these methods will be at the expense of energy resolution compared to the resolution from optimal filtering.

Once the spectrum and the live time are obtained, the spectrum is processed by fitting functions on peaks or on spectrum features. The spectrum processing allows to identify and separate the different contributions in the spectrum at characteristic energies:

- Lines from impurities, fluorescence or calibration lines
- Lines from the decay of the source in the absorber.

In the case of the presence of a continuous component of background, the spectrum processing allows to separate the peaks of the EC radionuclide or the alpha-emitting radionuclide inside the absorber from the background, and to determine the activity of the sample.

In the case of a beta-emitting radionuclide in the absorber, the continuous component of background is problematic because it is mixed with the beta spectrum and the spectrum processing cannot disentangle the background from the beta spectrum. The number of counts and the determined activity will be overestimated if the background events are not subtracted. There are two solutions. First, a MMC without source enclosed in the absorber can be used to monitor the background. However, this reference MMC must have the same absorber geometry as the other MMCs measuring the activity of the samples. The measured background can then be subtracted of the acquired spectra. The other solution is to simulate the background by Monte Carlo simulations. This solution requires a good knowledge of the detector geometry and its surrounding as well as a knowledge of the present radionuclides.

Section F: Literature

[1] Berger, M.J. et al. (2017), ESTAR, PSTAR, and ASTAR: Computer Programs for Calculating Stopping-Power and Range Tables for Electrons, Protons, and Helium Ions (version 2.0.1). [Online] Available: http://physics.nist.gov/Star [2022, November 21]. National Institute of Standards and Technology, Gaithersburg, MD.

[2] Hubbell, J.H. and Seltzer, S.M. (2004), Tables of X-Ray Mass Attenuation Coefficients and Mass Energy-Absorption Coefficients (version 1.4). [Online] Available: http://physics.nist.gov/xaamdi [2022, November 21]. National Institute of Standards and Technology, Gaithersburg, MD.

[3] Loidl, M., Rodrigues, M. and Mariam, R., “Measurement of the electron capture probabilities of ^{55}Fe with a metallic magnetic calorimeter”, *Applied Radiation and Isotopes*, vol. 134, 2018, doi: 10.1016/j.apradiso.2017.10.042.

[4] Loidl, M. et al., “First measurement of the beta spectrum of ^{241}Pu with a cryogenic detector, Applied Radiation and Isotopes”, *Applied Radiation and Isotopes*, vol. 68, no. 7-8, 2010, doi: 10.1016/j.apradiso.2009.11.054.

[5] Kossert, K. et al., “High precision measurement of the ^{151}Sm beta decay by means of a metallic magnetic calorimeter”, *Applied Radiation and Isotopes*, vol. 185, 2022, doi: 10.1016/j.apradiso.2022.110237.

[6] Ranitzsch, P. C.-O. et al., “Characterization of the ^{163}Ho Electron Capture Spectrum: A Step Towards the Electron Neutrino Mass Determination”, *Physical Review Letters*, vol. 119, no. 12, 2017, doi: 10.1103/PhysRevLett.119.122501.

[7] Mougeot, X., “Reliability of usual assumptions in the calculation of beta and neutrino spectra”, *Physical Review C*, vol. 91, no. 5, 2015, doi: 10.1103/PhysRevC.91.055504.

[8] Hayen, L. et al., “High precision analytical description of the allowed beta spectrum shape”, *Reviews of Modern Physics*, vol. 90, no. 1, 2018, doi: 10.1103/RevModPhys.90.015008.

[9] Paulsen, M., Kossert, K. and Beyer, J., “An unfolding algorithm for high resolution microcalorimetric beta spectrometry”, *Nuclear Instruments and Methods in Physics Research Section A: Accelerators, Spectrometers, Detectors and Associated Equipment*, vol. 953, 2020, doi: 10.1016/j.nima.2019.163128.

[10] Braß, M. and Haverkort, M.W., “Ab initio calculation of the electron capture spectrum of ^{163}Ho: Auger–Meitner decay into continuum states”, *New Journal of Physics*, vol. 22, 2020, doi: 10.1088/1367-2630/abac72.

[11] Fässler, A., Gastaldo, L. and Šimkovic, F., “Neutrino mass, electron capture, and the shake-off contributions”, *Physical Review C*, vol. 95, no. 4, 2017, doi: 10.1103/PhysRevC.95.045502.

[12] Particle Data Group, “Review of Particle Physics”, *Progress of Theoretical and Experimental Physics*, vol. 2022, no. 8, 2022, doi: 10.1093/ptep/ptac097.

[13] National Research Council of Canada. Metrology Research Centre. Ionizing Radiation Standards. “EGSnrc: software for Monte Carlo simulation of ionizing radiation”, National Research Council of Canada, 2021, doi: 10.4224/40001303.

[14] Landau, L.D., “On the Energy Loss of Fast Particles by Ionisation”, *Collected Papers of L.D. Landau*, 1965, doi: 10.1016/B978-0-08-010586-4.50061-4.

[15] Göggelmann, A. et al., “Study of muon-induced background in MMC detector arrays for the ECHo experiment”, *The European Physical Journal C*, vol. 81, no. 363, 2021, doi: 10.1140/epjc/s10052-021-09148-y.

[16] Budjáš, D. et al., “Highly sensitive gamma-spectrometers of GERDA for material screening: Part I”, *arXiv*, 2008, doi: 10.48550/ARXIV.0812.0723.

[17] Budjáš, D. et al., “Highly sensitive gamma-spectrometers of GERDA for material screening: Part II”, *arXiv*, 2008, doi: 10.48550/ARXIV.0812.0768.

[18] “Radiopurity Database”, *Underground Science and Low Radioactivity Techniques*, [Online] Available: http://radiopurity.in2p3.fr/ [2023, January 17].

[19] Göggelmann, A. et al., “Study of naturally occurring radionuclides in the ECHo set-up”, *The European Physical Journal C*, vol. 82, no. 139, 2022, doi: 10.1140/epjc/s10052-022-10112-7.

[20] Szymkowiak, A.E. et al., “Signal processing for microcalorimeters”, *Journal of Low Temperature Physic*s, vol. 93, 1993, doi: 10.1007/BF00693433.

[21] Kim, I. et al., “Trigger Study on the AMoRE-Pilot Detector”, Journal of Low Temperature Physics, vol. 193, 2018, doi: 10.1007/s10909-018-1973-5.

[22] Pommé S. et al., “Uncertainty of nuclear counting” 2015, *Metrologia* **52** S3, doi: 10.1088/0026-1394/52/3/S3.

[23] Hammann, R. et al., “Data reduction for a calorimetrically measured ^{163}Ho spectrum of the ECHo-1k experiment”, *The European Physical Journal C*, vol. 81, no. 963, 2021, doi: 10.1140/epjc/s10052-021-09763-9.

[24] PhD thesis, Göggelmann, A. “Background Studies for the ECHo Experiment”, 2022, doi: 10.15496/publikation-70662.